Computational Investigation of Ion Cyclotron Heating on Proto-MPEX

P. A. Piotrowicz,[1,2,a)] R. H. Goulding,[1] J. F. Caneses,[1] D. L. Green,[1] J. B. O. Caughman,[1] C. Lau,[1] J. Rapp,[1] and D. N. Ruzic[2]

[1)] *Oak Ridge National Laboratory, Oak Ridge, TN, 37830, USA*

[2)] *University of Illinois Urbana-Champaign, Urbana, IL, 61801, USA*

(Dated: 26 February 2019)

Ion cyclotron heating (ICH) on the Prototype Material Plasma Exposure eXperiment (Proto-MPEX) is to be accomplished using the "beach-heating" technique. Beach heating has not been previously demonstrated to efficiently heat core ions at the high electron density values present in Proto-MPEX. This work numerically investigates the wave propagation characteristics of the ICH region on Proto-MPEX to explore avenues for efficient core ion heating. The analysis reveals that finite electron temperature effects are required to predict core ion heating. Cold plasma dispersion analysis and full-wave simulations show that the inertial Alfvén wave (IAW) is restricted from coupling power into the core plasma because 1) the group velocity is too shallow for its energy to penetrate into the core before damping in the periphery, and 2) when operating in a magnetic field where $\omega/\omega_{ci} \gtrsim 0.7$ the IAW is cutoff from the core plasma by the Alfvén resonance. However, including kinetic effects shows that the kinetic Alfvén wave (KAW) can propagate in the electron temperature regime in Proto-MPEX. Full-wave simulations show that when the electron temperature is increased to $T_e > 2$ eV, and the edge electron density is sufficiently high $n_{e_{edge}} > 1 \times 10^{17}$ m^{-3}, ion power absorption in the core increases substantially ($\approx 25\%$ of total power). The increase in ion power absorption in the core is attributed to the propagation of the KAW. Calculations of electron and ion power absorption show that the electron heating is localized around the Alfvén resonance while the ion heating is localized at the fundamental ion cyclotron resonance.

Keywords: MPEX, Proto-MPEX, ion cyclotron heating, ion cyclotron resonance, plasma heating, beach heating, plasma waves, Alfvén wave, electron heating, full wave simulation, 3D antenna simulation

I. INTRODUCTION

Direct ion heating is expected to increase ion temperatures on the Prototype Material Plasma Exposure eXperiment (Proto-MPEX) to values of 30 eV or more[1]. In this regime, Proto-MPEX can simulate the effects in a fusion reactor divertor, in which ion temperature is expected to play an important role in the plasma-material interaction physics[2]. Ion heating on Proto-MPEX will be accomplished by launching a left-hand polarized wave from a region of high magnetic field to a region of decreasing magnetic field strength, where the wave encounters the ion cyclotron resonance. At the cyclotron resonance, the rotating electric field of the wave accelerates ions that are in phase with it and therefore leads to an increase in the perpendicular energy of the ions and damping of the wave[3,4]. Fig. 1 depicts a conceptual drawing of the wave propagation in this heating scenario. This ion heating technique is well known and is referred to as "beach heating". Beach heating has been demonstrated to heat ions efficiently on several devices including the B-66 stellarator

[a)] Electronic mail: ppiotr3@illinois.edu

in the 1960s[5], later on tandem mirrors such as Phaedrus[6] and Tara[7], and more recently on VASIMR VX-50[8]. The high electron density of Proto-MPEX make this a novel environment for beach heating. The electron density is an order of magnitude higher on Proto-MPEX than the devices this technique was previously demonstrated on. This work aims to show that a theoretical route to efficient core ion heating exists at such high electron density.

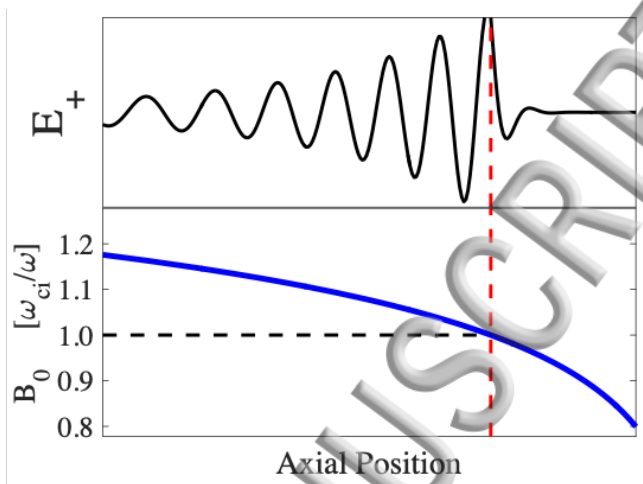

FIG. 1. Conceptual drawing of the wave propagation in a beach heating scenario.

Wave propagation in this regime has been studied across several areas of plasma science including the Earth's magnetosphere, fusion devices, and the solar corona. This regime has been studied in-depth on the LAPD device[9–12]. The wave of interest to the ICH region on Proto-MPEX is the shear Alfvén wave. This wave propagates on the slow wave branch of the dispersion relation and is classified in the literature into two limits of propagation corresponding to either cold or hot electrons and is typically sorted by comparing the Alfvén velocity to the thermal velocity of the electrons. With cold electrons ($v_{th_e} \ll v_A$) the wave propagates in the inertial regime and a cold plasma tensor can capture the propagation of this wave. However, when this wave propagates in a plasma with hotter electrons ($v_{th_e} \gg v_A$) the wave is said to propagate in the kinetic regime and a kinetic plasma tensor is required to describe the wave propagation. McVey[13] classifies the propagation of these waves by different means. The shear Alfvén wave in the inertial limit propagates on the low electron density side of the Alfvén resonance, or when the parallel index of refraction of the wave is greater than the S component of the Stix tensor ($n_\parallel^2 \geq S$), and the parallel phase velocity of the wave is greater than the electron thermal velocity of the wave ($v_{p_\parallel} \gg v_{th_e}$). McVey then describes the shear Alfvén wave in the kinetic regime to propagate on the high electron density side of the Alfvén resonance ($n_\parallel^2 \leq S$) and the parallel phase velocity of the wave is less than the electron thermal velocity of the wave ($v_{p_\parallel} \ll v_{th_e}$). Here we will refer to the shear Alfvén wave in the inertial regime as the inertial Alfén wave (IAW) and in the kinetic regime as the kinetic Alfvén wave (KAW).

Proto-MPEX can operate in a regime where both the IAW and the KAW propagate for magnetic field configurations where the driving frequency is near the ion cyclotron frequency ($\omega/\omega_{ci} > 0.7$). Proto-MPEX typically operates with an electron temperature between $T_e = 1$ and 6 eV such that the electron thermal velocity is approximately equivalent to the expected parallel phase velocity of the wave $v_{th_e} \approx \omega/k_\parallel$. Fig. 2 shows the Fourier spectrum from the ICH antenna on Proto-MPEX. The electron density gradient across the plasma column is such that the IAW wave propagates at the periphery of the plasma ($n_\parallel^2 \geq S$) and the KAW propagates in the core plasma ($n_\parallel^2 \leq S$). Therefore, for a constant magnetic field strength the $n_\parallel^2 = S$ contour lies across the plasma's electron density gradient and separates the regions where the IAW and the KAW can propagate. This contour is known as the

Alfvén resonance, and its presence has noteworthy consequences on the heating and wave propagation characteristics of the ion cyclotron heating (ICH) region. The Alfvén resonance location restricts the propagation of the KAW inside the plasma core and significant electron heating can take place along this contour[14,15]. Previous authors have described the heating of electrons in this layer due to mode conversion of the shear Alfvén wave (slow wave branch) to lower hybrid oscillations (fast wave branch)[16,17].

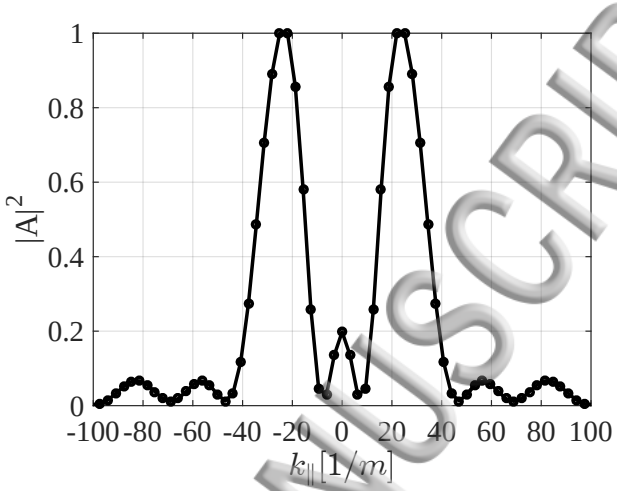

FIG. 2. Near field ($r = 3.6$ cm) vacuum spectrum of the B_y component of the RF magnetic field taken on the ZY plane excited by the ICH antenna.

In what follows, Section II describes the experimental configuration of the ICH region. Section III describes the 3D full-wave model used to investigate the wave propagation and heating in the ICH region. Section IV presents a dispersion analysis in the temperature regime where the IAW and KAW are expected to propagate. In this section we show the regions of propagation of the IAW and the KAW. The calculation of IAW's group velocity angle relative to the magnetic field is presented to show that in the geometry of Proto-MPEX this wave's energy is restricted from accessing the core plasma. Finally, Section V shows the results from a 3D full-wave model that predicts core ion heating when the electron temperature is raised to the level where the KAW is expected to propagate. Contours of power deposition are analyzed here to show the regions heated by the IAW and the KAW as well as the electron and ion heating due to these waves. Calculations of electron vs. ion heating in the ICH region are presented to show that the ions absorb most of the power deposited in the core plasma when $T_e > 2$ eV. A significant dependence on the value of the electron density at the edge ($n_{e_{edge}}$) of the plasma is shown, and no significant core heating is observed for $n_{e_{edge}} < 1 \times 10^{16}$ m^{-3}.

II. PROTO-MPEX ICH CONFIGURATION

Proto-MPEX is a linear plasma device operating at Oak Ridge National Lab (ORNL), on which the rf source concepts for MPEX are being developed and tested. Proto-MPEX uses a helicon antenna as the plasma source[18,19] to generate a plasma with electron densities of $n_e > 6 \times 10^{19}$ m^{-3} at the target plate. The plasma is then heated with microwaves and ICH to increase the electron and ion temperatures in the device to simulate the conditions of a fusion relevant divertor plasma[1,20,21]. For ICH experiments, the typical range of electron and ion temperatures are $T_e = 1$ to 3 eV and $T_i = 0$ to 12 eV respectively. For the simulations reported herein, the DC magnetic field at the ICH source and target location are approximately 1.2 T and 1.0 T respectively. The driving frequency of the ICH antenna

can be varied between 6 to 9 MHz, but for the purposes of the simulations presented here is set to 7.5 MHz. The ICH antenna is a 25 cm long, left-handed half-helical turn design[22].

A 2D schematic of the Proto-MPEX device is shown in Fig. 3. In this figure, on-axis magnetic field strength and flux line mapping in the 2D schematic are shown. The background magnetic field is produced with 12 magnetic field coils labeled as Coils 1-12 in the schematic. For the simulations reported in this work, the downstream coils are powered with 5600 A producing the magnetic field strength and flux mapping shown.

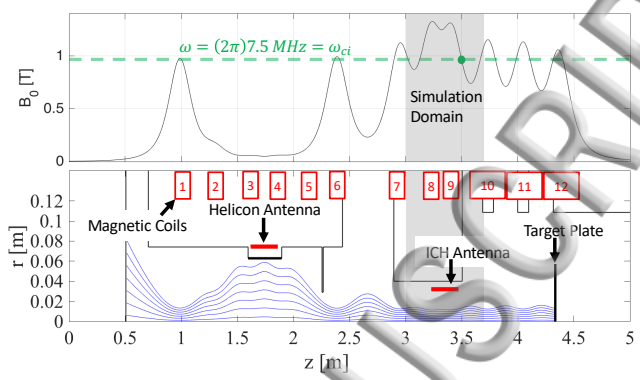

FIG. 3. On-axis magnetic field strength in Proto-MPEX for the magnetic configuration used in the simulations (top). Flux line mapping and a two dimensional schematic of Proto-MPEX (bottom). Magnetic Coils are depicted by the red boxes and labeled 1–12. The helicon antenna, the ICH antenna, and the target plate are labeled for reference.

III. FULL-WAVE MODEL

To model the plasma wave physics of the ICH region on Proto-MPEX, Maxwell's equations are solved in the frequency domain using the finite element analysis software COMSOL Multiphysics. A 3D geometry of the ICH antenna is used to solve for the electric field throughout the simulation domain. First, the simulation geometry used is described in Section III A. Next, in Section III B, a brief description of the magnetic field and electron density model used is discussed. Finally, the plasma tensor used to describe the linear plasma response to the applied rf is presented in Section III C.

A. Simulation Geometry

Fig. 4 shows a schematic of the simulation geometry. The coaxial feed where the port boundary condition is applied is labeled. The antenna feed is electrically connected to the center conductor of the feed coax while the antenna ground is electrically connected to the vacuum chamber. The ICH antenna geometry is replicated in COMSOL and is used for full-wave simulations of the ICH heating region in Proto-MPEX. The simulation is excited with a port boundary condition at the coaxial feed labeled in Fig. 4, which launches a coaxial TEM mode. The ICH antenna and coaxial feed structures are modeled as a perfect electrical conducting boundaries since we are not interested in the losses at the metal boundaries which are expected to be small compared to plasma loading. The currents along the ICH antenna are thus solved for self-consistently in the simulation. The simulation domain is divided into 3 regions with different material properties. The domain in which the antenna and coaxial structures are located has vacuum dielectric properties and is surrounded by the vacuum chamber which is also modeled as a perfect electrical conducting boundary. The region inside the vacuum region is the ceramic window, which

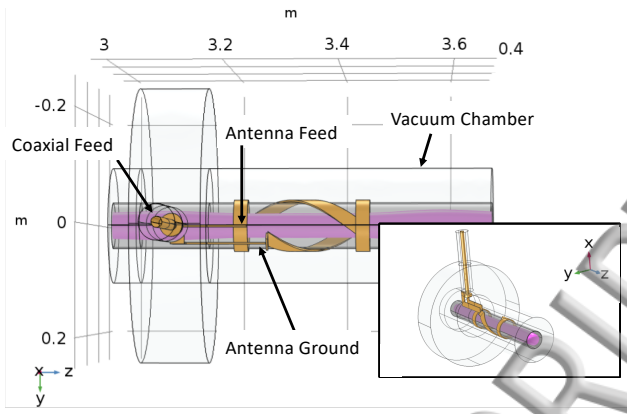

FIG. 4. Schematic of the ICH geometry used in COMSOL for the simulation. The YZ plane is shown and the ICH antenna, coaxial feed, antenna ground, and antenna feed are labeled. The antenna structure, feed strap, and ground strap is depicted as a golden color. The alumina window is shown in a dark grey region. Inside of the alumina window is the plasma volume where the bulk plasma is visualized by the pink contour. A 3D rendering of this geometry is shown in the lower right-hand side of the figure for clear visualization of the 3D geometry.

separates the antenna from the plasma column. This region has dielectric properties of alumina with a relative permittivity of $\epsilon_r = 10.2$, and a conductivity of $\sigma = 1 \times 10^{-12}$ S/m. Finally, inside the ceramic window region is the plasma region which has dielectric properties of a Maxwellian two-species (ions and electrons) plasma. The dielectric properties of the plasma are described in section III.C. The axial ends of the simulation are terminated with second order absorbing boundary conditions.

B. Simulation Inputs

The full-wave model requires inputs of magnetic field, electron density, and electron and ion temperatures. The magnetic field is calculated from Ampere's law in axisymmetric 2D using the experimental magnetic coil geometry shown in Fig. 3. The electron density is then defined as a function of magnetic flux as $n_e = (1 - \chi^a)^b + n_{e_{edge}}$, where χ is the flux function normalized such that plasma width corresponds to the measured plasma profile. The constants a and b are set to $a = 2$ and $b = 1.75$. This model for the electron density has been shown to capture the flux expansion of the plasma throughout Proto-MPEX[23]. For this analysis the peak electron density is set to $n_{e_{peak}} = 4 \times 10^{19}$ m^{-3}, the edge density is set to $n_{e_{edge}} = 10^{18}$ m^{-3}. The magnetic field for this simulation is solved for using a 2D asymmetric solution of Ampere's law given the current configuration shown in Fig. 3 and an imposed current on the magnet coils of $I_A = 5600$ A. Electron and ion temperatures are constant along the plasma column. The ion temperature is held at $T_i = 5$ eV, and electron temperature is scanned between $T_e = 0.6$ to 10 eV to show the effects that electron temperature plays on ion and electron core heating.

C. Plasma Tensor

The cold plasma tensor is only able to capture the physics of the inertial Alfvén wave (IAW). However, as will be discussed in Section IV, the Kinetic Alfvén wave (KAW) is expected to propagate in the Proto-MPEX ICH region. The ability to simulate both waves requires a plasma response that includes kinetic effects. A derivation of the Maxwellian kinetic plasma tensor can be found in Ref. 24. This tensor can then be simplified with the

finite Larmor radius approximation ($k_\perp r_{Ci} \ll 1$) to remove terms that include dispersion in the perpendicular direction. With this assumption, this model can capture the physics that allow the KAW to propagate[13]. Also, this formulation of the plasma response captures fundamental cyclotron and Landau damping of either electrons or ions. We note that this formulation of the plasma tensor will not capture any effects that are important near the harmonics of the cyclotron resonance, such as ion Bernstein wave propagation. Also, because this formulation relies on the finite Larmor radius approximation, the fast wave propagation near the Alfvén resonance may not be properly captured, as this wave undergoes an increase of $k_\perp$ towards infinity in the collisionless plasma limit. Because of the high electron density and low temperature, collisions are an important process in the Proto-MPEX plasma. The modifications to the kinetic tensor can be made using the Krook model. This collisional kinetic tensor was reported in Ref. 13 and is presented below.

The dielectric tensor used to simulate the plasma in Proto-MPEX is given by,

$$\boldsymbol{\epsilon}_r = \mathsf{Q}\mathsf{K}\mathsf{Q}^T, \tag{1}$$

where,

$$\mathsf{K} = \begin{bmatrix} S & -iD & 0 \\ iD & S & 0 \\ 0 & 0 & P \end{bmatrix}, \tag{2}$$

and Q is the rotation matrix to bring the z-axis component of K parallel to the magnetic field. The elements of K are

$$P = 1 - \sum_i \frac{\omega_{pi}^2}{(k_\parallel v_{th_i})^2} Z'(\xi_0)\beta^{-1}, \tag{3}$$

$$S = \frac{1}{2}(R + L), \tag{4}$$

$$D = \frac{1}{2}(R - L), \tag{5}$$

where

$$R = 1 + \sum_i \frac{\omega_{pi}^2}{\omega k_\parallel v_{th_i}} Z(\xi_1), \tag{6}$$

$$L = 1 + \sum_i \frac{\omega_{pi}^2}{\omega k_\parallel v_{th_i}} Z(\xi_{-1}), \tag{7}$$

$$\beta = \left(1 + \frac{i\nu_i}{k_\parallel \nu_i} Z(\xi_0)\right), \tag{8}$$

$$\xi_n = \frac{\omega + n\omega_{ci} + i\nu_i}{k_\parallel v_{th_i}}. \tag{9}$$

In Eqs. 3–9, $Z(\xi_n)$ is the plasma dispersion function, and $k_\parallel$ is the parallel wave number of the propagating wave. The collision, plasma, and cyclotron frequency of species i are denoted as ν_i, ω_{pi}, and ω_{ci} respectively. The thermal velocity of species i is v_{th_i}. Eqs. 6–9 describe a Maxwellian plasma with collisional damping. Coulomb collisions for both electrons and ions are calculated from the specified n_e and T_e. The electron collision frequency also has an addition of electron-neutral collisions with D_2. The electron-neutral collisions are calculated assuming a background neutral gas density of $n_0 = 3.2 \times 10^{18}$ m^{-3}, which is estimated from baratron measurements in the ICH region. Eqs. 6–9 are dispersive in the direction parallel to the magnetic field and require knowledge of $k_\parallel$. This is a non-local parameter and can be handled properly through using an all-orders spectral method[25,26]. However, for the purposes of this paper, $k_\parallel$ was approximated to be a constant dependant on the peak of the ICH antenna spectrum. For the ICH antenna used in this study the spectral peak for the $m = -1$ azimuthal mode is $k_\parallel \approx 20$ m^{-1}, and this will be the value used for $k_\parallel$ in the dielectric tensor[22].

IV. DISPERSION ANALYSIS

Understanding the dispersive properties of the plasma column is critical to interpreting full-wave simulations. The dispersion relation can be formulated by solving a 0D Helmholtz equation using the dielectric tensor given by Eq. 2. Assuming knowledge of the parallel wave number, $k_\parallel$, the solutions to the dispersion relation are a bi-quadratic equation to which the approximations of the two roots are given by

$$k^2_{\perp_{FW}} = \frac{(k_0^2 R - k_\parallel^2)(k_0^2 L - k_\parallel^2)}{k_0^2 S - k_\parallel^2}, \tag{10}$$

and

$$k^2_{\perp_{SW}} = \frac{P}{S}(k_0^2 S - k_\parallel^2). \tag{11}$$

With Eqs. 10 and 11, we can now understand the perpendicular propagation characteristics of the waves that have an parallel wave number driven by the ICH antenna geometry. The perpendicular wave number of the wave solved for by Eqs. 10 and 11 is a complex quantity. The real part gives the perpendicular wave number while the imaginary part gives the inverse of the damping length. With the dispersion relation, the propagation characteristics of the slow and fast waves can be mapped out to help interpret results from the full-wave simulation. Both the IAW and KAW are found to propagate on the slow-wave branch of the dispersion relation, and therefore, only this branch is analyzed. Lower-hybrid oscillations were described to be efficient sources of electron heating at the Alfvén resonance in Ref. 17, which analyzed the VASIMR beach heating scenario. These lower hybrid oscillations are described by the fast-wave branch of the dispersion relation. While typically the slow-wave branch of the dispersion relation contains larger $k_\perp$ than the fast-wave branch, near the Alfvén resonance the slow-wave branch experiences a decrease in $k_\perp$ toward zero and the fast-wave branch's $k_\perp$ increases towards infinity. Therefore, the two branches of the dispersion relation reach a confluence near the Alfvén resonance, which could lead to efficient mode conversion between the two branches[17], and therefore strong electron heating at the Alfvén resonance.

The regions of propagation of the IAW and the KAW are discussed in Section IV A. In Section IV B we discuss how electron temperature affects the wave propagation of the IAW and KAW. Next, a discussion of the energy access of the IAW to the core plasma is presented in Section IV C where we show that the IAW is restricted to the periphery of the plasma due to the small group velocity angle relative to the magnetic field.

A. Regions of Propagation

To help interpret the results from the full-wave simulation, we first solve the dispersion relation to understand the propagation characteristics of the plasma waves of interest. The relevant contours in the ICH region are the Alfvén resonance ($n_\parallel^2 = S$) and the ion cyclotron resonance ($\omega_{ci} = \omega$). The ion cyclotron resonance acts to strongly damp left-hand polarized waves and transfer the wave's energy to heat ions. The Alfvén resonance acts to cutoff the IAW and KAW, therefore separating the regions of propagation of both waves. As explained in Section I the IAW propagates on the low electron density side of the plasma column, the KAW propagates on the high electron density side at values of electron temperature that allow the electron thermal velocity to exceed the axial phase velocity of the wave. However, Proto-MPEX's ICH antenna operates in a regime where the thermal velocity is close to the parallel phase velocity of the wave and therefore both waves are expected to play a role in the heating.

Fig. 5 shows a 2D schematic of the ICH region with the relevant contours drawn. The magnetic field in this schematic is the same one as depicted in Fig. 3. The relevant contours that are depicted in Fig. 5 are the fundamental ion cyclotron resonance ($\omega = (2\pi)7.5$ MHz),

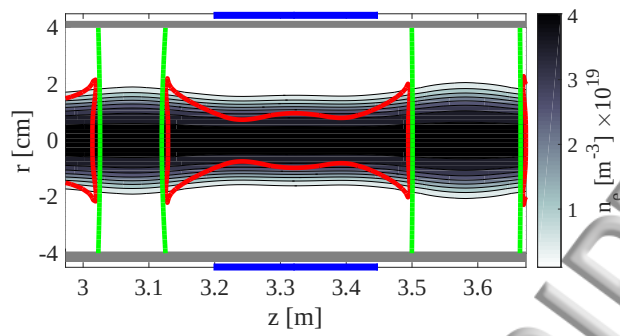

FIG. 5. Schematic of the ICH region in Proto-MPEX. The electron density profile in the ICH region is shown. The green contours represent the magnetic field value at which the ion cyclotron resonance at 7.5 MHz driving frequency exists. The red contours are locations of the Alfvén resonance at $k_\parallel = 20$ m^{-1}. The ICH antenna is represented by the solid blue line and is separated from the plasma by an alumina tube which is represented by the grey line.

depicted by the solid green lines, and the Alfvén resonance, which is depicted by the red contour lines. The contours of the Alfvén resonance have a dependence on the electron density, magnetic field strength, and parallel wave number. For the simulation of interest in this paper, the Alfvén resonance acts to restrict access of the IAW from the core plasma and confine the KAW to the core plasma.

B. Electron Temperature Effects

Electron temperature affects the propagation characteristics of both the IAW and KAW. However, in our regime the KAW is effected more than the IAW by electron temperature. Fig. 6 shows the calculation of the real part of $k_\perp$ as a function of electron density from Eq. 11. The electron density covers the range expected across the plasma column in the Proto-MPEX ICH region. The calculation is made for several values of T_e relevant to current and future experimental scenarios in Proto-MPEX.

The dispersion calculation presented shows that the IAW is cutoff from the core plasma at the Alfvén resonance, which occurs for electron density values of $n_e \approx 1 \times 10^{19}$ m^{-3} at a magnetic field strength of $B_0 = 1.2$ T. The plot shows that Proto-MPEX operates in a regime where the KAW begins to propagate. The IAW does not propagate when T_e is very large, such that $v_{th_e} \gg \omega/k_\parallel$. However, for the conditions of Proto-MPEX this regime of T_e is not accessible and therefore Proto-MPEX operates in a temperature regime where the physics of both the IAW and KAW are relevant. Therefore, a cold plasma model cannot be used to accurately model the ICH region, and the effect of electron temperature is necessary to describe the wave propagation in the ICH region. In Section V we investigate the effect of electron temperature on predicted core ion power absorption from the 3D numerical simulations.

C. IAW Group Velocity Restriction

The group velocity of an electromagnetic wave describes the direction in which the wave's energy propagates. In materials with complex dielectric properties, such as a plasma, the group velocity of the wave is not necessarily parallel to its phase velocity. To understand the propagation of the plasma wave's energy we utilize an expression for the angle between the phase velocity and the group velocity, α, which is written as

$$\tan\alpha = -\frac{1}{k}\frac{\partial k}{\partial \theta}, \tag{12}$$

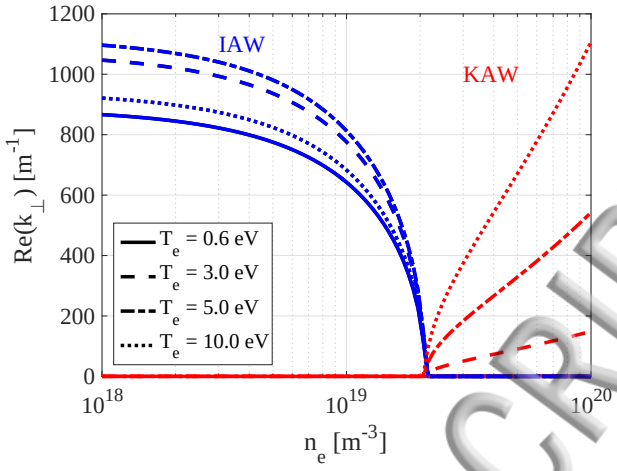

FIG. 6. Dispersion calculations of $\mathrm{Re}(k_\perp)$ as a function of electron density for several values of electron temperature. The inertial Alfvén wave (IAW) is depicted by the blue curves and it is calculated from the slow-wave branch of the dispersion relation when $S < n_\parallel^2$. The kinetic Afvén wave (KAW) is depicted by the red curves and it is calculated from the slow-wave branch of the dispersion relation when $S > n_\parallel^2$. The dispersion relation is solved assuming $k_\parallel = 20$ m^{-1}, $\omega = (2\pi)7.5$ MHz, $B_0 = 1.2$ T.

and can be found in Ref. 27. The dispersion relation for the IAW is given by Eq. 11. For simplicity we reduce the STIX tensor components in Eq. 11 to those of the cold plasma tensor. Full-wave simulations do not indicate significant temperature effect on the group velocity of the IAW, so for the purpose of this section this assumption will be sufficient. The angle between the phase velocity and the magnetic field is defined as $\tan\theta = k_\perp/k_\parallel$. Eq. 12 requires us to express the dispersion relation in terms of $k(\theta)$ as

$$k^2 = -\frac{Sk_0^2\omega_{pe}^2}{-\omega_{pe}^2\cos^2\theta + S\omega^2\sin^2\theta}. \tag{13}$$

The angle between the group velocity and the phase velocity is then

$$\alpha = \tan^{-1}\left[-\frac{1}{k}\frac{(S\omega^2+\omega_{pe}^2)\cos\theta\sin\theta}{Sk_0^2\omega_{pe}^2}\left(\frac{Sk_0\omega_{pe}^2}{\omega_{pe}^2\cos^2\theta - S\omega^2\sin^2\theta}\right)^{3/2}\right]. \tag{14}$$

Therefore, the angle between the group velocity and the magnetic field is $\Psi = \alpha + \theta$.

Fig. 7 shows that before the IAW encounters the Alfvén resonance it propagates at a narrow group velocity angle with respect to the magnetic field. This acts to restrict the energy of this wave to the periphery of the plasma column and therefore prevents its energy from penetrating into the core plasma for Proto-MPEX's current geometry and operating frequency range. This is the primary reason that the IAW cannot couple power into the plasma core to heat ions there. The simulation results in the following section will show that the power deposition of the IAW is restricted to the periphery of the plasma, and power that is coupled to the core plasma is due to the excitation of the KAW.

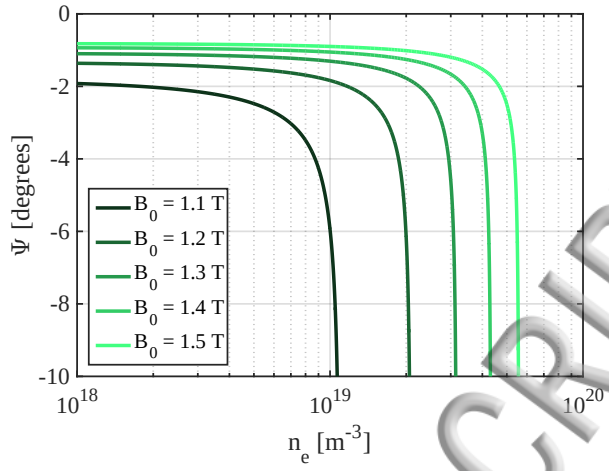

FIG. 7. Calculations of the angle of the IAW group velocity from the magnetic field (Ψ), as a function of electron density for several values of magnetic field strength ($B_0 = 1.1$–1.5 T).

V. SIMULATION RESULT

In this section, we show the results of the 3D full-wave simulation described in Section III. First, we present a calculation for electron and ion power absorption and show contour plots of power deposition in the ICH heating region for each species. Next, we discuss the effect of increasing the electron temperature in the simulation from $T_e = 0.6$ eV to $T_e = 10$ eV. We show that by increasing the electron temperature the simulation predicts increased core ion heating. Contours of ion power deposition are presented at several values of electron temperature to show that plasma heating associated with the IAW is located in the periphery of the plasma and that core heating is due to the excitation of the KAW. Finally, the dependence of core ion heating on edge electron density is presented along with a discussion on the excitation mechanisms of the KAW.

A. Electron vs. Ion Heating

Past experiments on Proto-MPEX[22] and the Tara tandem mirror device[7] showed evidence of direct electron heating during ICH beach heating. The ICH antenna on Proto-MPEX is designed to directly heat the ions, therefore, it is useful to predict which species in the plasma are being heated by the rf to optimize the heating configuration for ion heating. The main diagnostics used to measure ion heating in the plasma are IR thermography[28] of the target plate and Ar II spectroscopy[22]. The IR thermography gives a 2D view of the power deposition on the target plate. However, this measurement cannot distinguish if the increased power to the target is due to increased ion energy in the bulk plasma or to increased electron temperatures. The Ar II spectroscopy directly measures the ion temperature. Since this is a line integrated measurement there is uncertainty in the radial location contributing to the ion temperature measurements. Therefore, calculations of the energy absorbed by the electrons vs. the ions can help explain the experimental measurements, as well as optimize the configuration for ion heating.

The power deposition mechanisms that are captured by the dielectric tensor used in the model are collisionless Landau damping, fundamental cyclotron resonance absorption, and collisional damping. For the case of collisional damping the collision frequency is calculated from Coulomb collisions for both electrons and ions, and electron-neutral collisions with deuterium molecules ($n_0 = 3.2 \times 10^{18}$ m^{-3}). The electron collision frequency in Proto-

MPEX is shown to be very large ($\nu_{ei} > \omega$)[19], and therefore contributes significantly to the power absorption. Non-collisional electron heating (Landau damping) is also important in the ICH region because the ICH antenna operates such that $v_{p_\parallel} \approx v_{th_e}$. The Alfvén resonance is a location where strong electron heating is predicted to occur by both Landau and collisional damping[14–17,29]. The lower hybrid resonance layer in our geometry is located physically close to the ion cyclotron resonance at a lower magnetic field, enhanced electron heating can be expected near this layer. The ions are expected to be heated primarily by the resonant absorption of the wave at the fundamental ion cyclotron resonance. The power deposited to electrons and ions can be found by separately calculating the electron and ion currents from the expected conductivity due to each species. The conductivity due to each species is calculated from the Stix tensor, while only including the species of interest in the summation. Then using Ohm's law, the power absorbed by the electrons and ions independently is,

$$P_{e,i} = \mathbf{J}_{e,i} \cdot \mathbf{E}, \tag{15}$$

where

$$\mathbf{J}_{e,i} = \boldsymbol{\sigma}_{e,i} \cdot \mathbf{E}, \tag{16}$$

$$\boldsymbol{\sigma}_{e,i} = i\omega\epsilon_0 \left(\mathsf{I} - \mathsf{K}_{e,i}\right). \tag{17}$$

$\mathbf{J}_{e,i}$ is the induced current and $\boldsymbol{\sigma}_{e,i}$ is the conductivity tensor associated with either electrons or ions. $\mathsf{K}_{e,i}$ is the plasma tensor given by Eq. 2 but retaining only the terms in the summations that represent the species of interest.

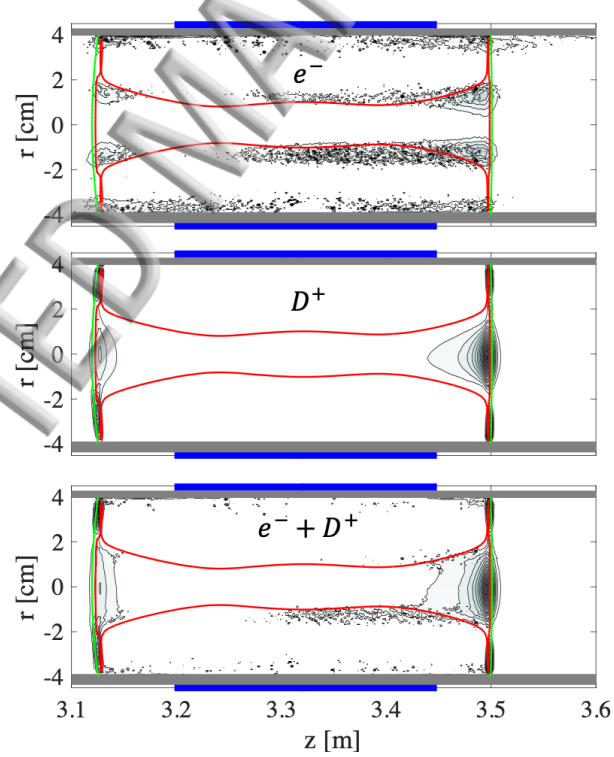

FIG. 8. YZ plane contours of the normalized rf power absorption in the plasma by electrons only (top), ions only (middle), and by both ions and electrons (bottom). These calculations of the rf power absorption are from the 3D full-wave simulation presented in Section III for an electron temperature of $T_e = 2.1$ eV. Contours of the Alfvén $k_\parallel^2 = (20\ \mathrm{m}^{-1})^2 = k_0^2 S$ are depicted by the red line, while contours of the fundamental ion cyclotron resonance $B_{IC} = \omega m_i/q$ are depicted by the green lines.

Fig. 8 shows the contours from the calculation of the rf power absorption by the species present in the plasma. Interpreting these contours reveals the dominant power absorption mechanisms during ICH experiments. The ion power absorption is predominantly located at the fundamental cyclotron resonance location. The electron power absorption seems to occur in the periphery of the plasma column and at the Alfvén resonance and there is enhancement of electron power deposition near the ion cyclotron resonance which we attribute to the presence of the lower hybrid resonance. Since electron absorption in Proto-MPEX is not negligible, there is an advantage to keeping the ion cyclotron resonance location in close proximity to the ICH antenna if efficient ion heating is desired. The proximity of the ion cyclotron resonance prevents the rf wave from being damped by the electrons before it reaches the resonance location, where it couples power to the ions. If electron heating is desired, moving the ion cyclotron resonance away from the plasma may be a viable route to heating electrons with low frequency rf.

B. Electron Temperature Effect on Core Ion Heating

The effect of electron temperature on the ion heating efficiency in the core plasma, defined as $\chi < 0.6$, is important to understand to design an ICH system for MPEX. The IAW is not expected to contribute significantly to heating the plasma core due to the group velocity restriction explained in Section IV C. Also, for the magnetic field and driving frequency used, the IAW is cutoff from the core by the Alfvén resonance. Increasing the magnetic field at the ICH antenna can act to remove the Alfvén resonance from the plasma column. However, this does not increase the core power deposition from the IAW because of the proximity of the ion cyclotron resonance and the group velocity restriction on this wave. Therefore, observations of core ion heating are attributed to coupling to the KAW. Since the excitation of the KAW has an electron temperature dependence as shown in Fig. 6, the core ion heating efficiency of the ICH is also expected to have a dependence on electron temperature.

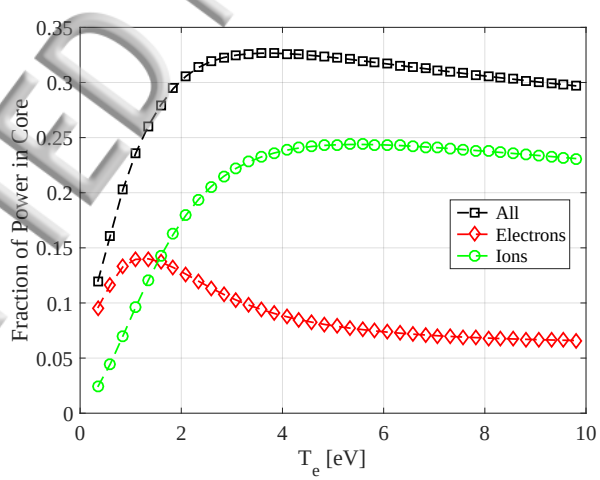

FIG. 9. Integrated core power deposition for both ions and electrons (black squares), ions only (green circles), and electrons only (red diamonds) is normalized to the total power deposited in the simulation domain plotted as a function of electron temperature. The input parameters for this 3D full-wave simulation are described in Section III.

Fig. 9 shows the integrated power absorbed in the core plasma, and the division of this absorbed power by each species (electrons and ions) as a function of electron temperature. The core ion power deposition increases with electron temperature until $T_e \approx 5$ eV where it begins to slightly decline. The core electron power deposition is at its maximum at

$T_e \approx 1$ eV. This is most likely due to a balance between excitation of the KAW in the core (which is responsible for heating electrons in the core near the Alfvén resonance) and a decreasing collision frequency. At electron temperatures of $T_e > 2$ eV, rf absorption by the ions dominates the absorption by the electrons, and for an electron temperature $T_e > 4$ eV we calculate $\approx 80\%$ of the power delivered to the core is attributed to ion heating.

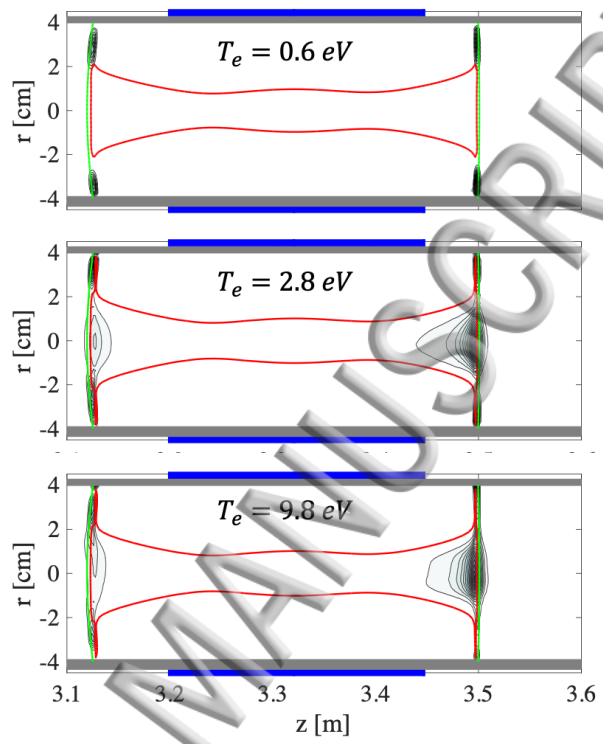

FIG. 10. YZ plane contours of the normalized rf power absorbed by the ions (P_i) shown for increasing values of electron temperature $T_e = 0.6$ eV (top), $T_e = 2.1$ eV (middle), and $T_e = 9.8$ eV (bottom). Contours of the Alfvén $k_\parallel^2 = (20\ m^{-1})^2 = k_0^2 S$ are depicted by the red line, while contours of the fundamental ion cyclotron resonance $B_{IC} = \omega m_i/q$ are depicted by the green lines.

Fig. 10 shows where the ion power is deposited in the simulation domain as the electron temperature varies from a cold plasma ($T_e = 0.6$ eV) to a plasma with higher electron temperature ($T_e > 2$ eV). The Alfvén resonance is depicted by the red contour line and, as was explained in Section IV A, this boundary acts to separate the region where the IAW can propagate from the region where the KAW propagates. The green contours are the location of the fundamental cyclotron resonance, and we see that the ion power absorption takes place near the resonance. For the case of colder plasmas, we see that the ion power absorption is only present in the periphery of the plasma column in the region where the IAW propagates. As T_e is increased above 2 eV, power absorption in the core plasma begins to increase. This power absorption region is separated from the absorption in the periphery by the Alfvén resonance, which provides further evidence that the power absorption in the periphery of the plasma is attributed to the IAW and the power absorption in the core plasma is attributed to the KAW.

C. Dependence on Edge Electron Density

Fig. 11 shows the fraction of power in the core plasma coupled to electrons, ions, and both species as a function of edge electron density ($n_{e_{edge}}$). This figure shows a significant

increase in core power deposition when the edge electron density is increased up until $n_{e_{edge}} \approx 2 \times 10^{18}$ m^{-3}, then a slight decrease in coupling is observed. Values of edge electron density above $n_e > 10^{18}$ m^{-3} begin to affect the propagation characteristics of the KAW in the core plasma and are unlikely to be experimentally relevant. However, the numerical effect of the higher edge electron density on core power deposition is enlightening for understanding the coupling of rf power to the KAW. Below $n_{e_{edge}} < 1 \times 10^{17}$ m^{-3} the amount of core power deposition becomes less than 5%, while $n_{e_{edge}} = 1 \times 10^{18}$ m^{-3} shows $\approx 30\%$ of the total power being coupled to the core. The edge electron density profile in Proto-MPEX is not well known, but it seems an important consideration for coupling ICH power into the core plasma.

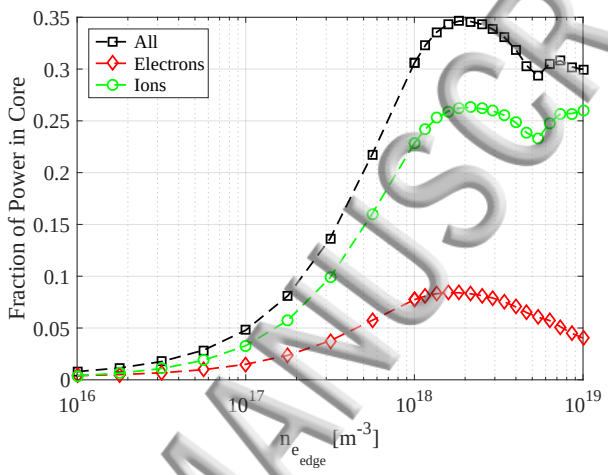

FIG. 11. Integrated core power deposition for both ions and electrons (black squares), ions only (green circles), and electrons only (red diamonds) is normalized to the total power deposited in the simulation domain plotted as a function of electron density in the edge ($n_{e_{edge}}$). Electron temperature is set to $T_e = 5$ eV, the other input parameters in the simulation are described in Section III.

The excitation mechanisms of the KAW are important to understand in order to optimize the ICH antenna for core ion heating. The candidate excitation mechanisms for the KAW are either from evanescent near fields under the antenna or transition of the IAW to the KAW. When considering transition of the IAW as the excitation mechanism of the KAW the energy access of the IAW becomes an important consideration. The group velocity of the IAW is almost parallel to the magnetic field for the field strength directly under the antenna. Therefore, the most likely location for the transition to occur would be near the ion cyclotron resonance. This is because the group velocity of the IAW becomes increasingly perpendicular to the magnetic field as the wave approaches the Alfvén resonance, and the Alfvén resonance is moving to lower values of electron density as the wave approaches the ion cyclotron resonance, this trend is shown in Fig. 7. When considering evanescent excitation of the KAW, the size of the evanescent gap, the region of plasma density where $n_\parallel^2 \geq S$), would determine the efficiency of coupling rf power into the KAW. Changing the inner diameter of the ceramic tube effectively changes the evanescent gap size in the simulation domain. Reducing the evanescent gap by 2 cm increased power coupling by $\approx 5\%$. The increase in coupling was linear and not very effective. If the KAW was excited through evanescent fields directly under the antenna, an exponential increase in power coupling would be expected.

The dependence on edge electron density shown in Fig. 11 supports the idea that the excitation mechanism of the KAW is via a transition that occurs near the ion cyclotron resonance. The idea is that at higher values of electron densities, up until the Alfvén resonance layer, the group velocity of the IAW becomes increasingly perpendicular. Exploring this

mechanism further, and confirming the physics of the dependence on edge electron density is outside of the scope of this paper and will be left for future work.

VI. DISCUSSION AND CONCLUSION

The propagation characteristics of the waves in the ICH region in Proto-MPEX have been investigated numerically with dispersion analysis and a 3D full wave model. This full-wave model made use of a simplified dielectric tensor derived by assuming a linear response of a plasma with a Maxwellian energy distribution function of both the ions and the electrons. The addition of the kinetic effects into the plasma tensor was shown to predict core ion heating. Analysis of the dispersion properties in the ICH region shows that both the IAW and the KAW can propagate in the Proto-MPEX plasma. However, the IAW cannot couple power into the plasma core due to the narrow-angle of the group velocity and the Alfvén resonance restricting its access to the core. This consideration is important for the efficiency of the beach heating on Proto-MPEX since the wave is launched at the periphery of the plasma and cannot access the core if the ion cyclotron resonance is located in close proximity to the antenna as is the case in the current experimental configuration. However, the excitation of the KAW is possible in the temperature regime of Proto-MPEX and opens an avenue for efficient heating of core ions.

The simulation results show that when the edge electron density is sufficiently high ($n_e > 1 \times 10^{17}$ m^{-3}), and the electron temperature is increased to where the KAW is expected to propagate ($T_e > 2$ eV), the core power deposition increases significantly (5%–30% of the total power). These numerical results demonstrate that kinetic effects are required to capture the physics of the ICH system on Proto-MPEX. This result is unexpected at such low values of electron temperature where cold plasma physics is typically sufficient to capture wave-propagation.

Since both electrons and ions are expected to absorb rf energy in Proto-MPEX a question of interest is the split between heating electrons and ions in the core. To answer this question, contours of power absorbed by the ions vs. the power absorbed by the electrons are presented to show the locations where this heating is occurring. The ion heating primarily occurs at the ion cyclotron resonance, whereas the electron heating occurs either at the periphery of the plasma column or at the Alfvén resonance. The most significant contribution to core electron heating occurs from the interaction of the plasma wave with the Alfvén resonance. This can be attributed to either Landau damping at this resonance[29] or mode conversion to lower hybrid oscillations[16]. Then, integrated core power from the full-wave calculations shows that above $T_e > 4$ eV the ions absorb ($\approx 80\%$) of the power coupled to the core or ($\gtrsim 20\%$ of the total power). Therefore, this work numerically demonstrates a theoretical route to efficient core ion heating on Proto-MPEX.

VII. ACKNOWLEDGEMENTS

This material is based on the work supported by the U.S. Department of Energy, Office of Science, Office of Fusion Energy Sciences, under Contract No. DEAC05-00OR22725. This manuscript was authored by UT-Battelle, LLC, under Contract No. DE-AC05-00OR22725 with the U.S. Department of Energy. The U.S. Government retains and the publisher, by accepting the article for publication, acknowledges that the U.S. Government retains a non-exclusive, paid-up, irrevocable, world-wide license to publish or reproduce the published form of this manuscript, or allow others to do so, for U.S. Government purposes. The Department of Energy will provide public access to these results of federally sponsored research in accordance with the DOE Public Access Plan (http://energy.gov/downloads/doe-public-access-plan).

VIII. REFERENCES

[1] J. Rapp, T. M. Biewer, T. S. Bigelow, J. Caughman, R. C. Duckworth, R. J. Ellis, D. R. Giuliano, R. H. Goulding, D. Hillis, R. Howard, *et al.*, "The development of the material plasma exposure experiment," IEEE Transactions on Plasma Science **44**, 3456–3464 (2016).

[2] P. Stangeby, "The chodura sheath for angles of a few degrees between the magnetic field and the surface of divertor targets and limiters," Nuclear Fusion **52**, 083012 (2012).

[3] J. Lehane and F. Paoloni, "Hydromagnetic wave propagation in inhomogeneous magnetic fields," Plasma Physics **12**, 823 (1970).

[4] Y. Yasaka, R. Majeski, J. Browning, N. Hershkowitz, and D. Roberts, "ICRF heating with mode control provided by a rotating field antenna," Nuclear Fusion **28**, 1765 (1988).

[5] T. H. Stix and R. W. Palladino, "Observation of Ion Cyclotron Waves," Physics of Fluids **641** (1960), 10.1063/1.1706099.

[6] D. R. Roberts and N. Hershkowitz, "Enhanced Slow-Wave Beach Heating of Mirror Plasmas with Two-Ion species," Physics of Fluids B: Plasma Physics **4**, 1475–1485 (1992).

[7] S. N. Golovato, K. Brau, J. Casey, J. Coleman, M. J. Gerver, W. Guss, G. Hallock, S. Horne, J. Irby, R. Kumazawa, J. Kesner, B. Lane, J. Machuzak, T. Moran, R. Myer, R. S. Post, E. Sevillano, D. K. Smith, J. D. Sullivan, R. Torti, L. Wang, Y. Yasaka, X. Z. Yao, and J. Zielinski, "Plasma production and heating in a tandem mirror central cell by radio-frequency waves in the ion cyclotron frequency range," Physics of Fluids **31**, 3744–3753 (1988).

[8] E. A. Bering, F. R. Díaz, J. P. Squire, T. W. Glover, M. D. Carter, G. E. McCaskill, B. W. Longmier, M. S. Brukardt, W. J. Chancery, and V. T. Jacobson, "Observations of single-pass ion cyclotron heating in a trans-sonic flowing plasma," Physics of Plasmas **17** (2010), 10.1063/1.3389205.

[9] W. Gekelman, S. Vincena, and D. Leneman, "Experimental observations of shear Alfvén waves generated by narrow current channels," Plasma Physics and Controlled Fusion **39**, A101 (1997).

[10] C. Kletzing, S. Bounds, J. Martin-Hiner, W. Gekelman, and C. Mitchell, "Measurements of the shear Alfvén wave dispersion for finite perpendicular wave number," Physical review letters **90**, 035004 (2003).

[11] W. Gekelman, S. Vincena, B. Van Compernolle, G. Morales, J. Maggs, P. Pribyl, and T. Carter, "The many faces of shear Alfvén waves," Physics of Plasmas **18**, 055501 (2011).

[12] S. Vincena, W. Gekelman, and J. Maggs, "Shear Alfvén waves in a magnetic beach and the roles of electron and ion damping," Physics of Plasmas **8**, 3884–3896 (2001).

[13] B. McVey, "ICRF antenna coupling theory for a cylindrically stratified plasma," (1984).

[14] L. Chen and A. Hasegawa, "Plasma heating by spatial resonance of Alfvén wave," The Physics of Fluids **17**, 1399–1403 (1974).

[15] A. Hasegawa and L. Chen, "Theory of plasma heating by nonlinear excitation of lower hybrid resonance," The Physics of Fluids **18**, 1321–1326 (1975).

[16] A. Timofeev, "On the influence of Alfvén resonance on ion cyclotron resonance heating," Plasma Physics Reports **40**, 1–13 (2014).

[17] A. V. Timofeev, "On RF heating of inhomogeneous collisional plasma under ion-cyclotron resonance conditions," Plasma Physics Reports **41**, 873–881 (2015).

[18] R. H. Goulding, J. B. O. Caughman, J. Rapp, T. M. Biewer, T. S. Bigelow, I. H. Campbell, J. F. Caneses, D. Donovan, N. Kafle, E. H. Martin, H. B. Ray, G. C. Shaw, and M. A. Showers, "Progress in the development of a high power helicon plasma source for the materials plasma exposure experiment," Fusion Science and Technology **72**, 588–594 (2017).

[19] P. A. Piotrowicz, J. F. Caneses, D. L. Green, R. H. Goulding, C. Lau, J. B. O. Caughman, J. Rapp, and D. N. Ruzic, "Helicon normal modes in proto-mpex," Plasma Sources Science and Technology (2018).

[20] J. Rapp, T. M. Biewer, T. Bigelow, J. B. O. Caughman, R. Duckworth, D. Giuliano, R. H. Goulding, D. L. Hillis, R. Howard, R. J. Ellis, T. Lessard, J. D. Lore, A. Lumsdaine, E. Martin, W. D. Mcginnis, S. J. Meitner, L. W. Owen, H. Ray, G. Shaw, and V. Varma, "The Material Plasma Exposure eXperiment MPEX : pre-design , development and testing of source concept," (2015).

[21] J. Rapp, T. Biewer, T. Bigelow, J. Caneses, J. Caughman, S. Diem, R. Goulding, R. Isler, A. Lumsdaine, C. Beers, T. Bjorholm, C. Bradley, J. Canik, D. Donovan, R. Duckworth, R. Ellis, V. Graves, D. Giuliano, D. Green, D. Hillis, R. Howard, N. Kafle, Y. Katoh, A. Lasa, T. Lessard, E. H. Martin, S. Meitner, G.-N. Luo, W. McGinnis, L. Owen, H. Ray, G. Shaw, M. Showers, V. Varma, and the MPEX team, "Developing the science and technology for the material plasma exposure experiment," Nuclear Fusion **57**, 116001 (2017).

[22] C. J. Beers, R. H. Goulding, R. C. Isler, E. H. Martin, T. M. Biewer, J. F. Caneses, J. B. O. Caughman, N. Kafle, and J. Rapp, "Helicon plasma ion temperature measurements and observed ion cyclotron heating in proto-MPEX," Physics of Plasmas **25**, 1–9 (2018).

[23] P. A. Piotrowicz, J. F. Caneses, M. Showers, D. L. Green, R. H. Goulding, J. B. O. Caughman, T. M. Biewer, J. Rapp, and D. N. Ruzic, "Direct measurement of the transition from edge to core power coupling in a light-ion helicon source," Physics of Plasmas (2018).

[24] M. Brambilla, *Kinetic Theory of Plasma Waves: Homogeneous Plasmas*, International Series of Monogr (Clarendon Press, 1998).

[25] E. Jaeger, L. Berry, and D. Batchelor, "Full-wave calculation of sheared poloidal flow driven by high-harmonic ion bernstein waves in tokamak plasmas," Physics of Plasmas **7**, 3319–3329 (2000).

[26] D. Green and L. Berry, "Iterative addition of parallel temperature effects to finite-difference simulation of radio-frequency wave propagation in plasmas," Computer Physics Communications **185**, 736–743 (2014).
[27] D. G. Swanson, *Plasma waves*, 2nd ed. (Institute of Physics Publishing, Philadelphia).
[28] M. Showers, T. M. Biewer, J. B. O. Caughman, D. C. Donovan, R. H. Goulding, and J. Rapp, "Heat flux estimates of power balance on Proto-MPEX with IR imaging," Review of Scientific Instruments **87**, 11D412 (2016).
[29] T. H. Stix, *Waves in Plasmas*, edited by 1 (AIP-Press, 1992) pp. XIII, 566.

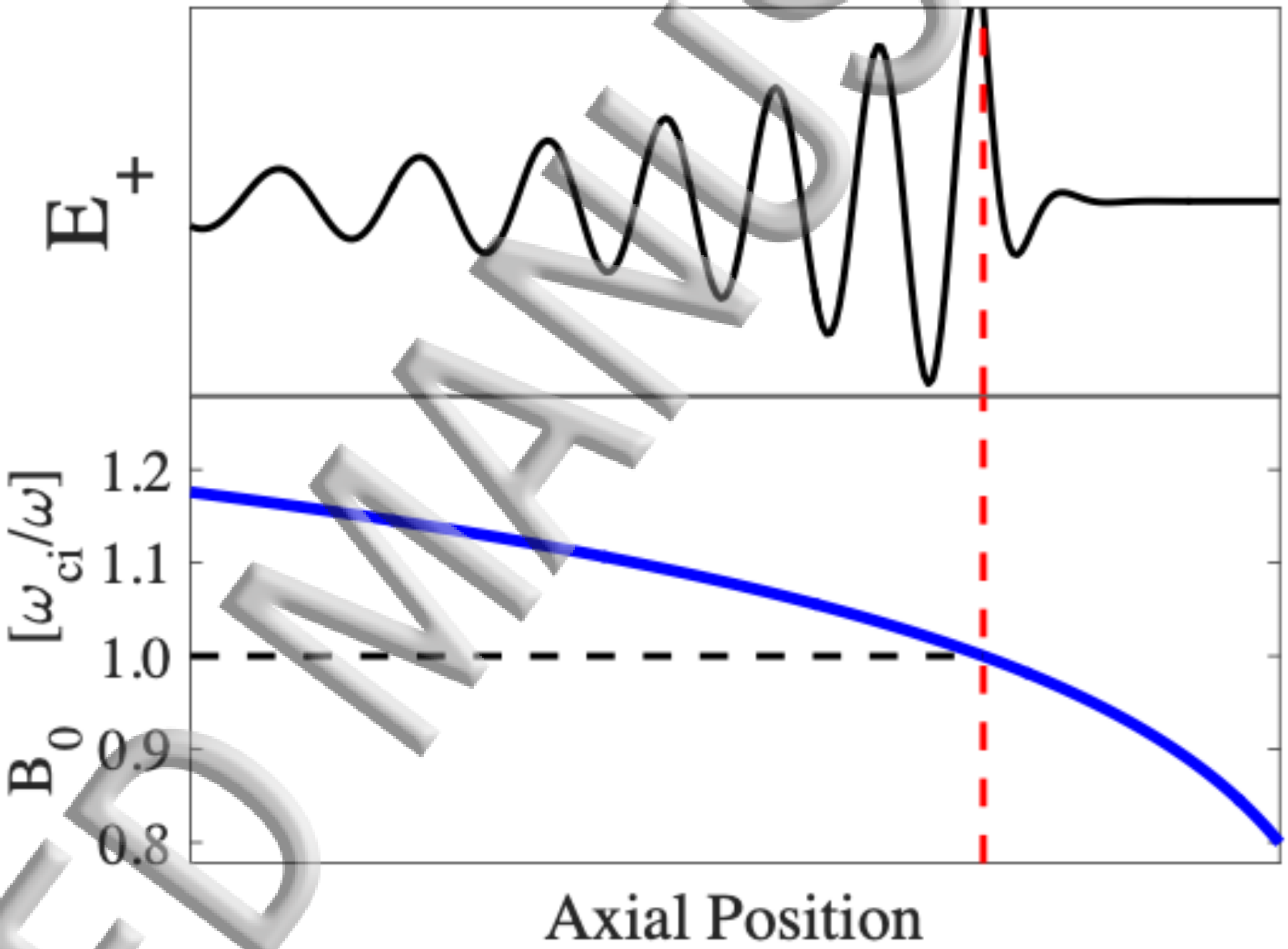
E+
1.2
1.1
1.0
0.9
0.8
[ωci/ω]
B0
Axial Position

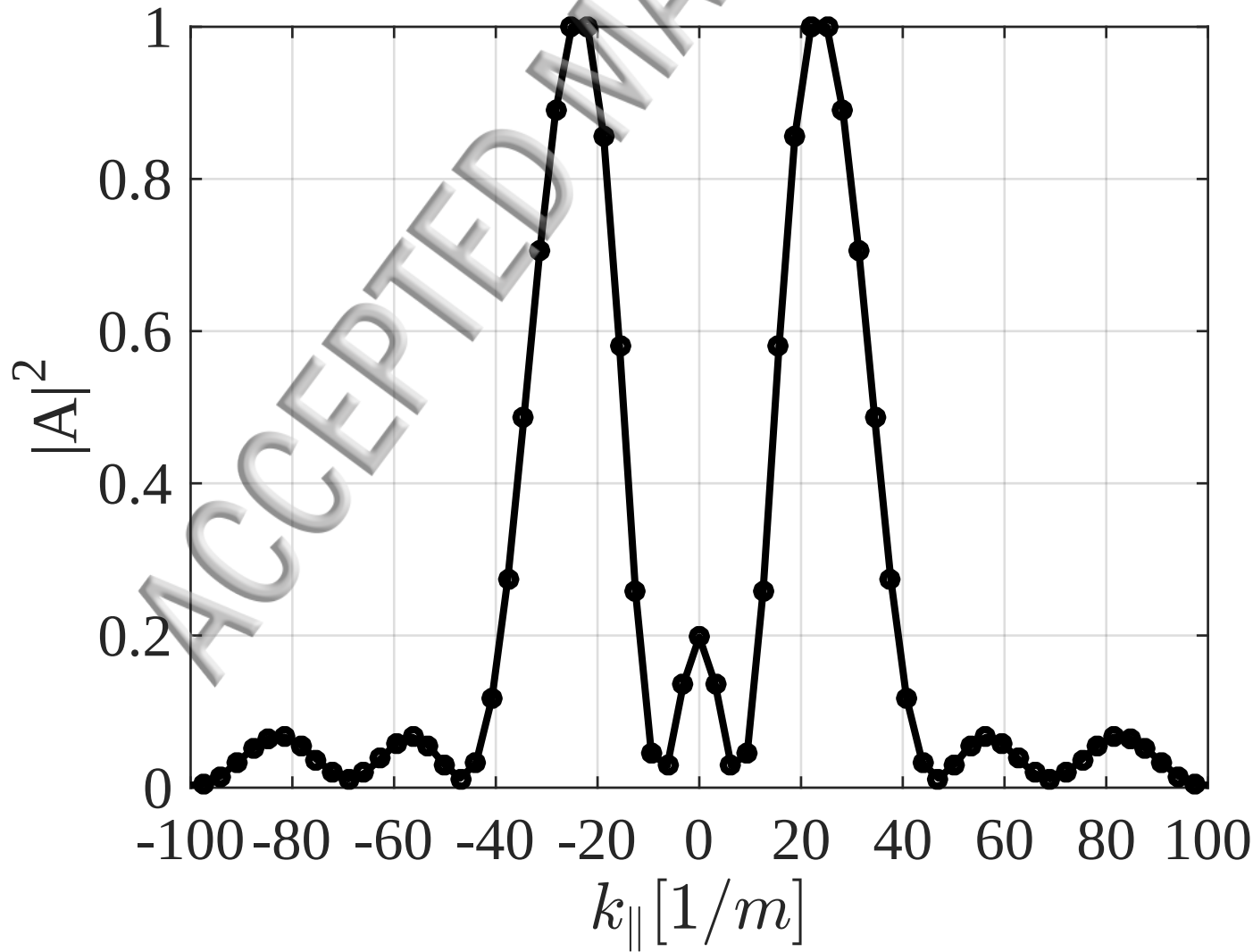

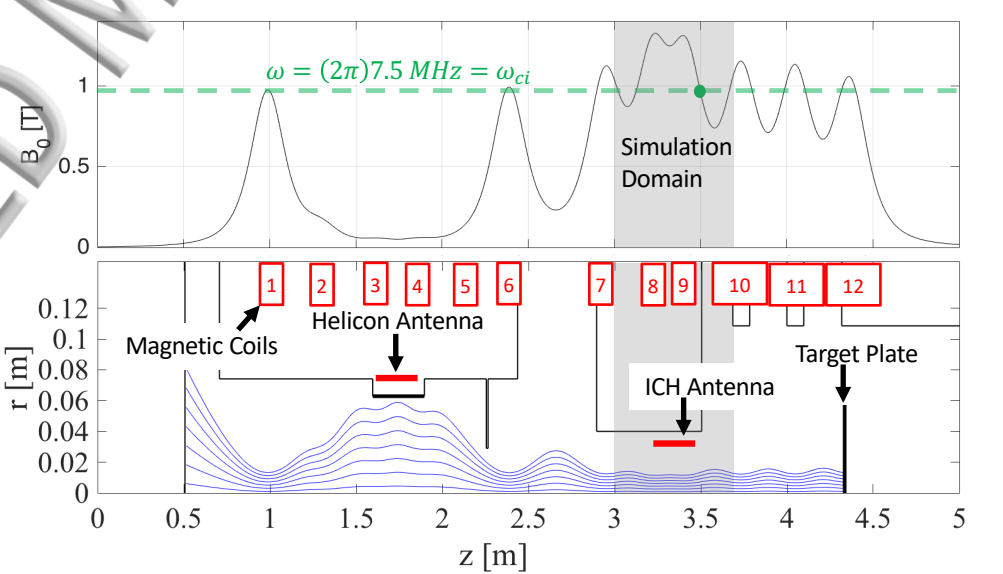
$\omega = (2\pi)7.5\ MHz = \omega_{ci}$
B_0 [T]
1
0.5
0
Simulation Domain
1
2
3
4
5
6
7
8
9
10
11
12
Magnetic Coils
Helicon Antenna
ICH Antenna
Target Plate
r [m]
0.12
0.1
0.08
0.06
0.04
0.02
0
0
0.5
1
1.5
2
2.5
3
3.5
4
4.5
5
z [m]

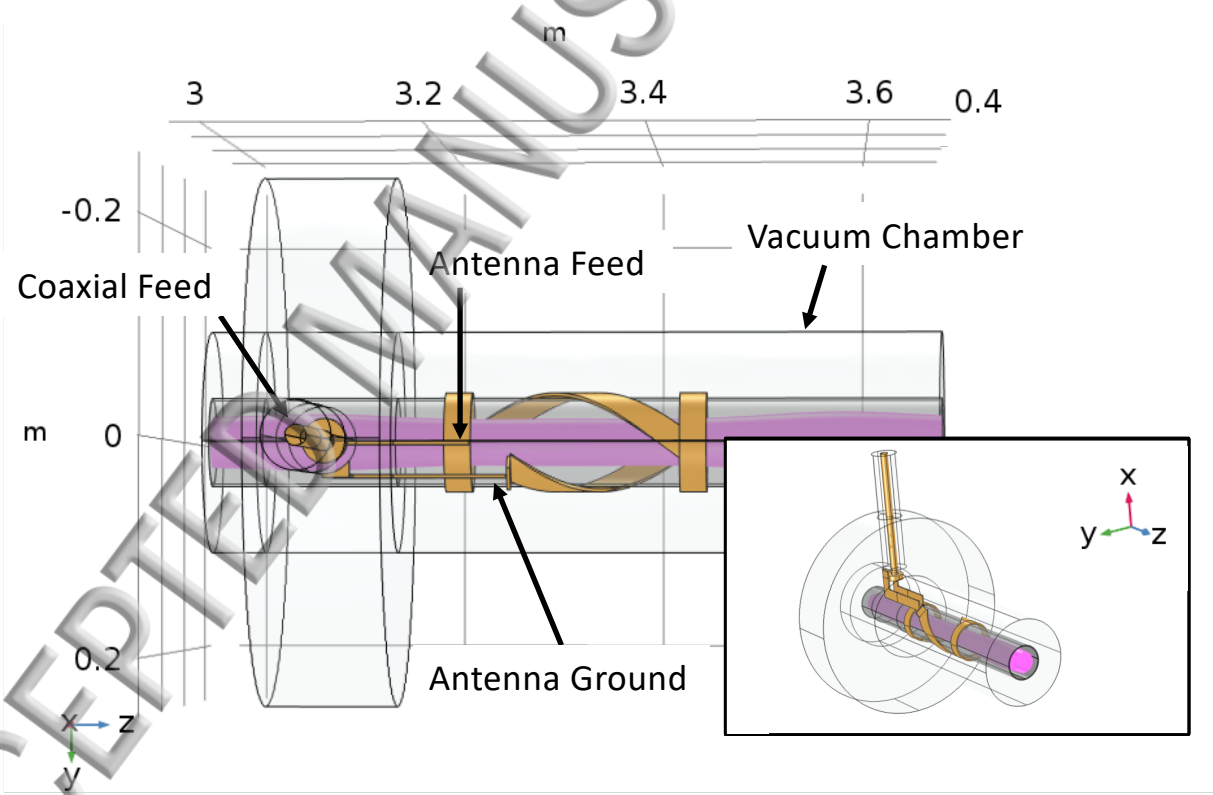

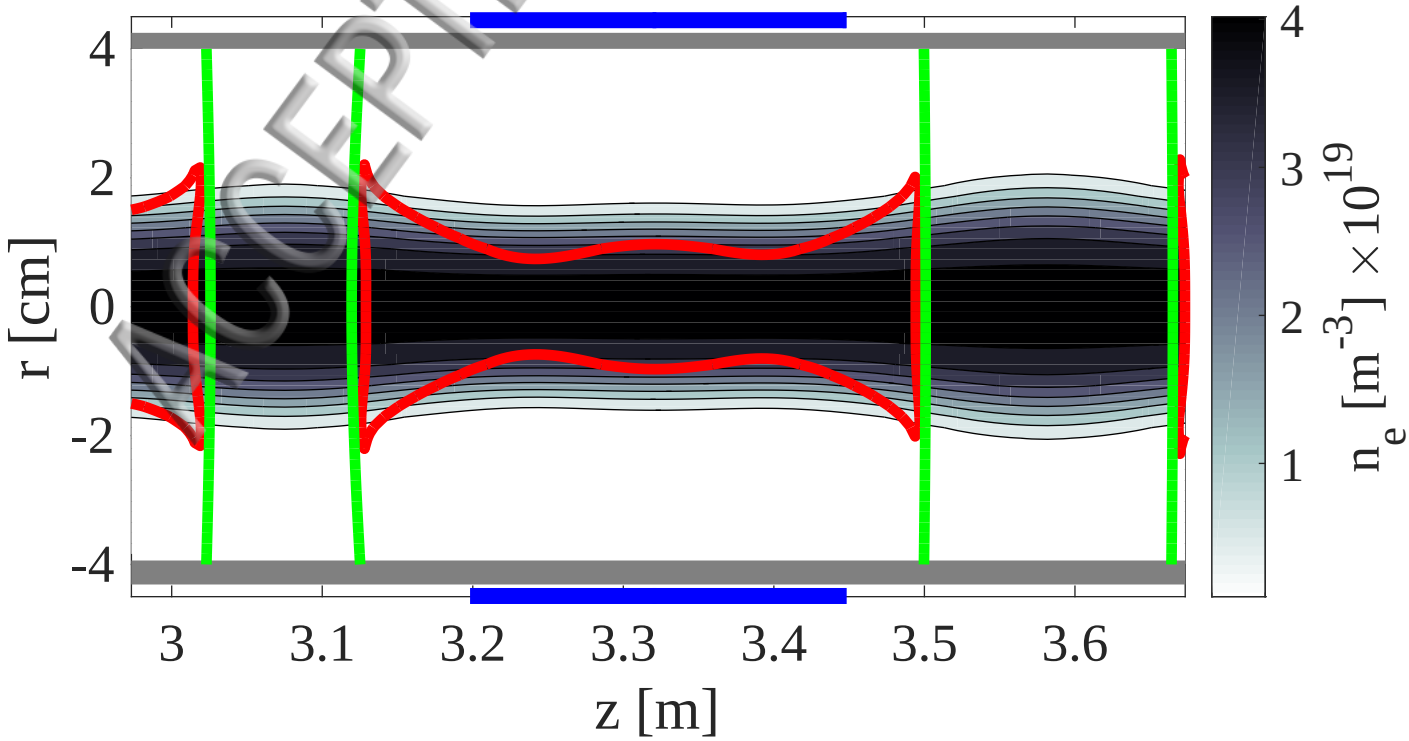

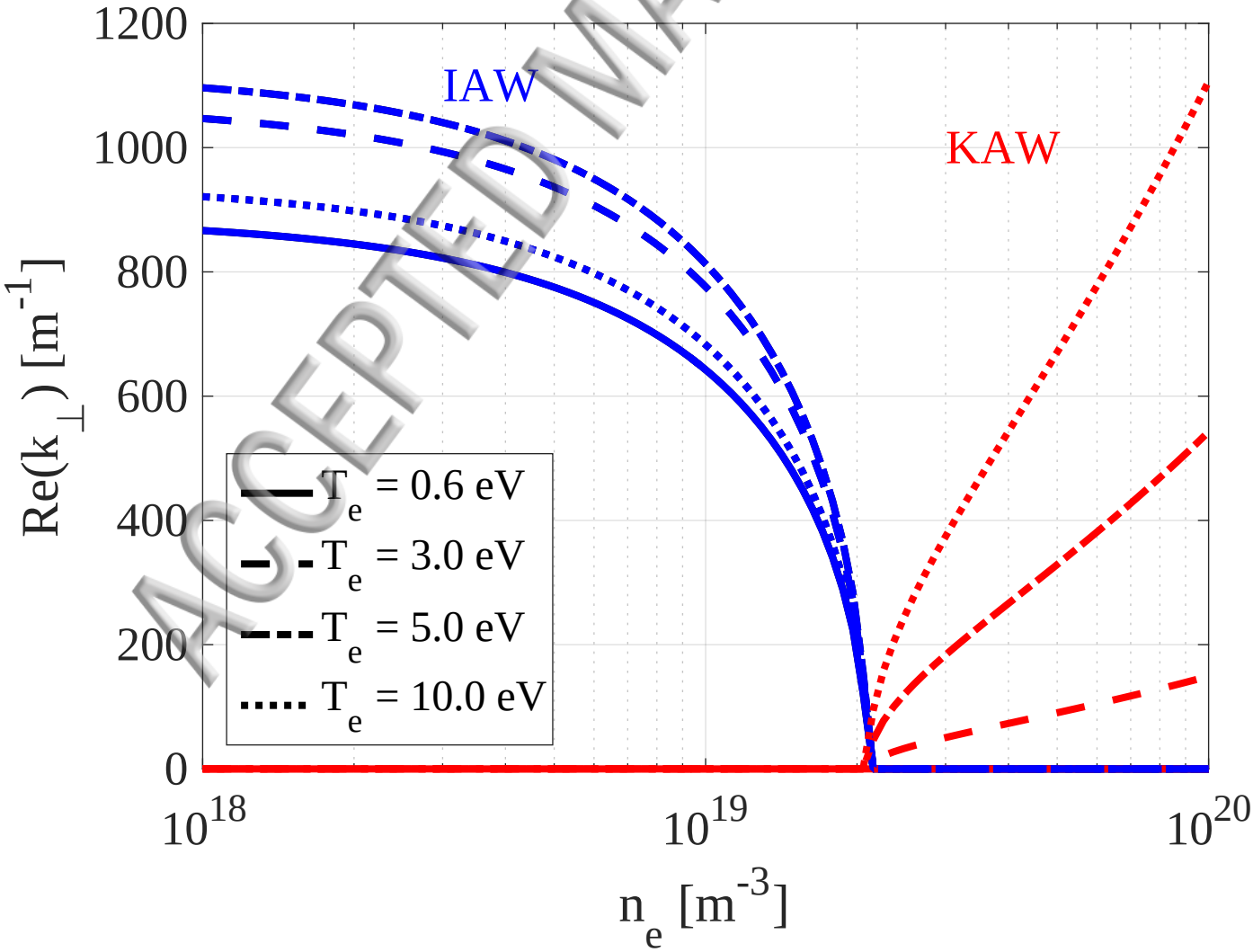

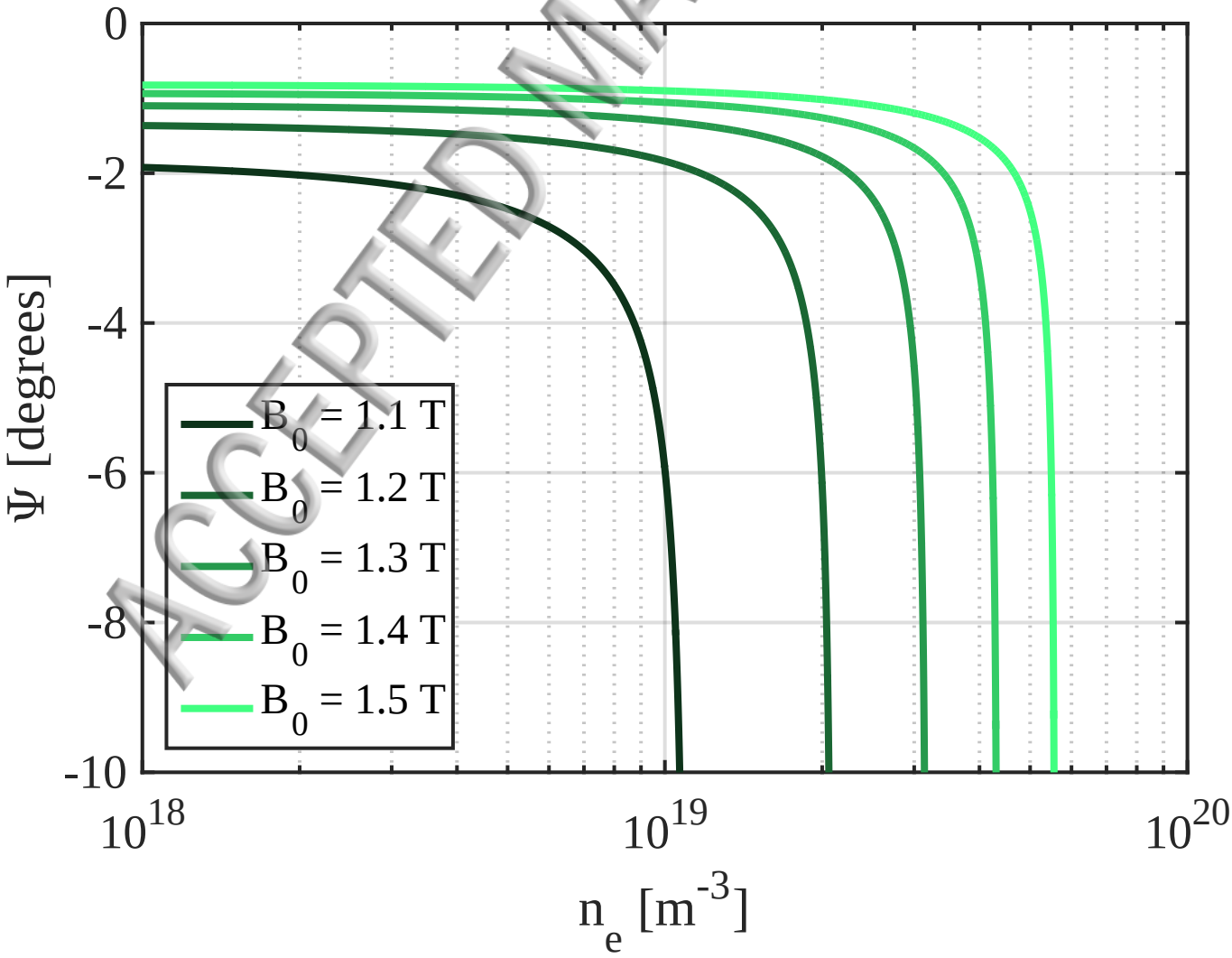

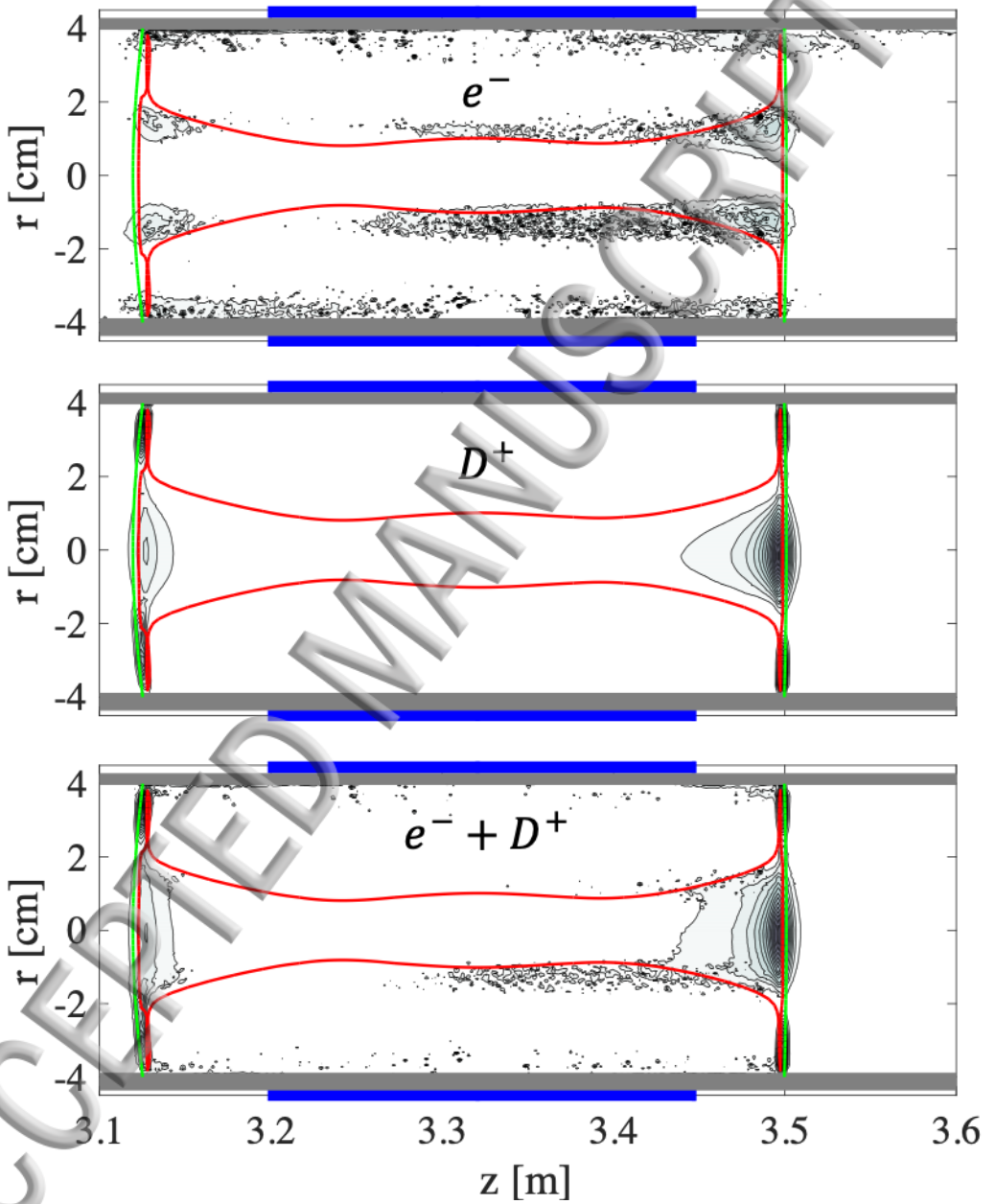

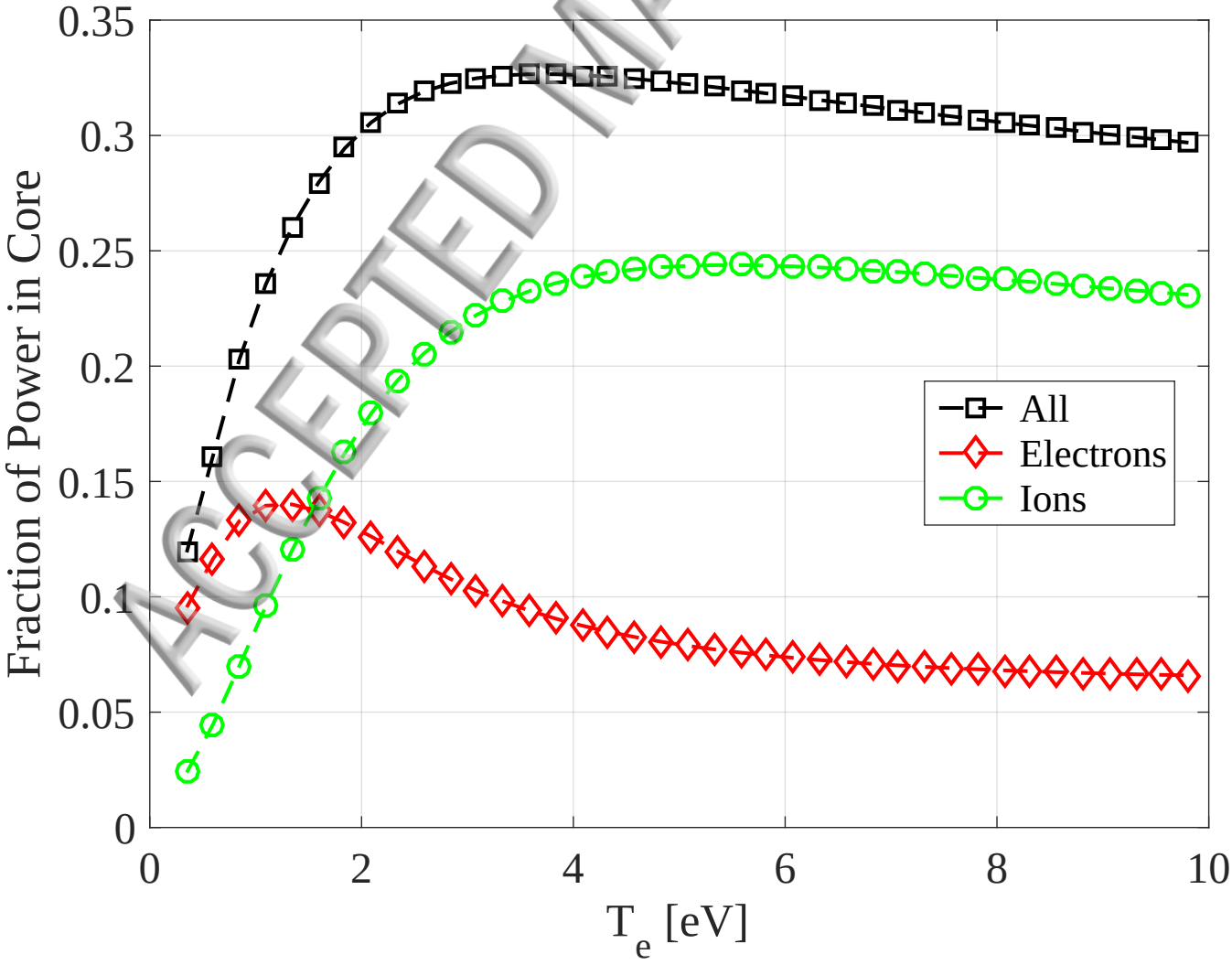

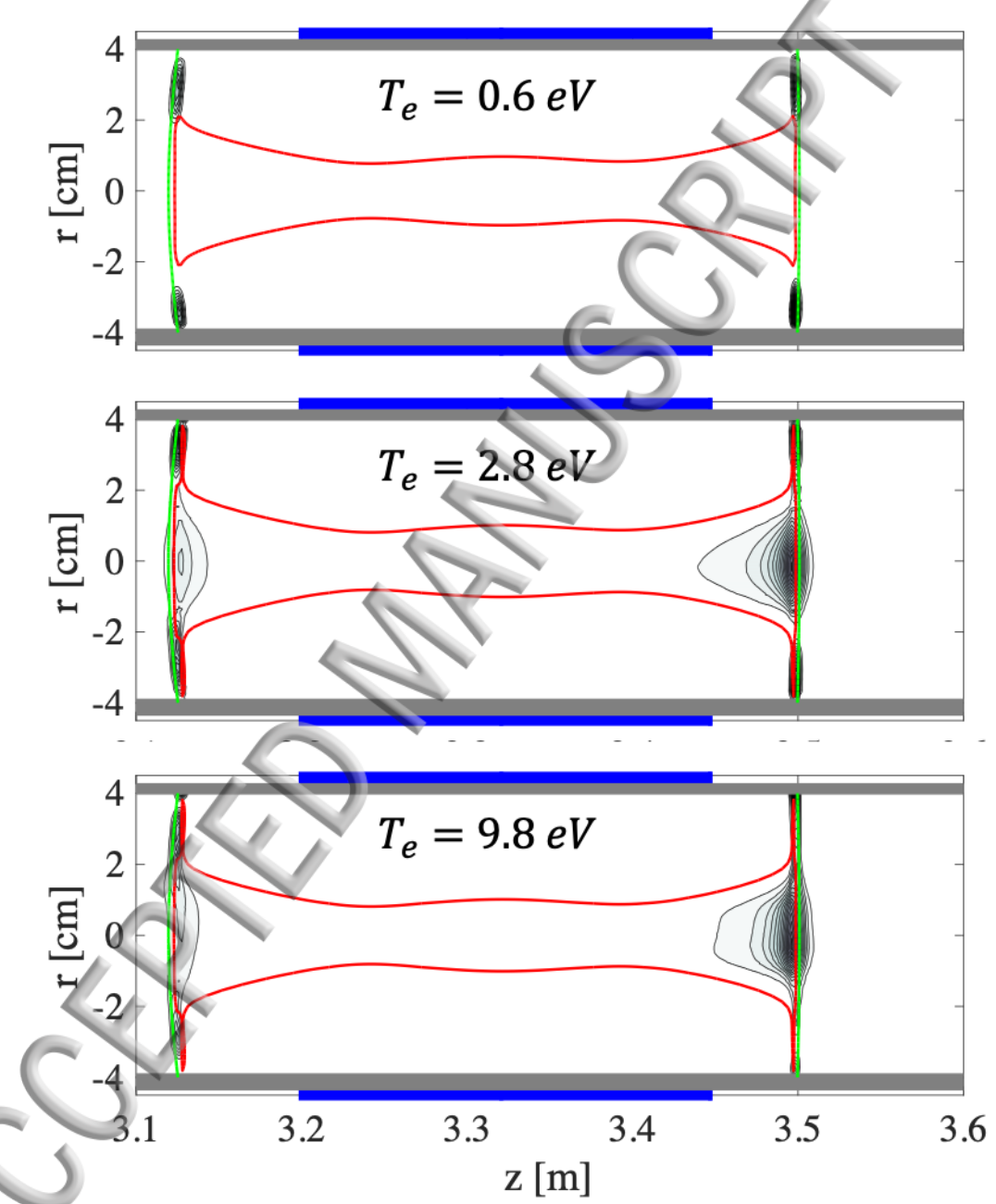

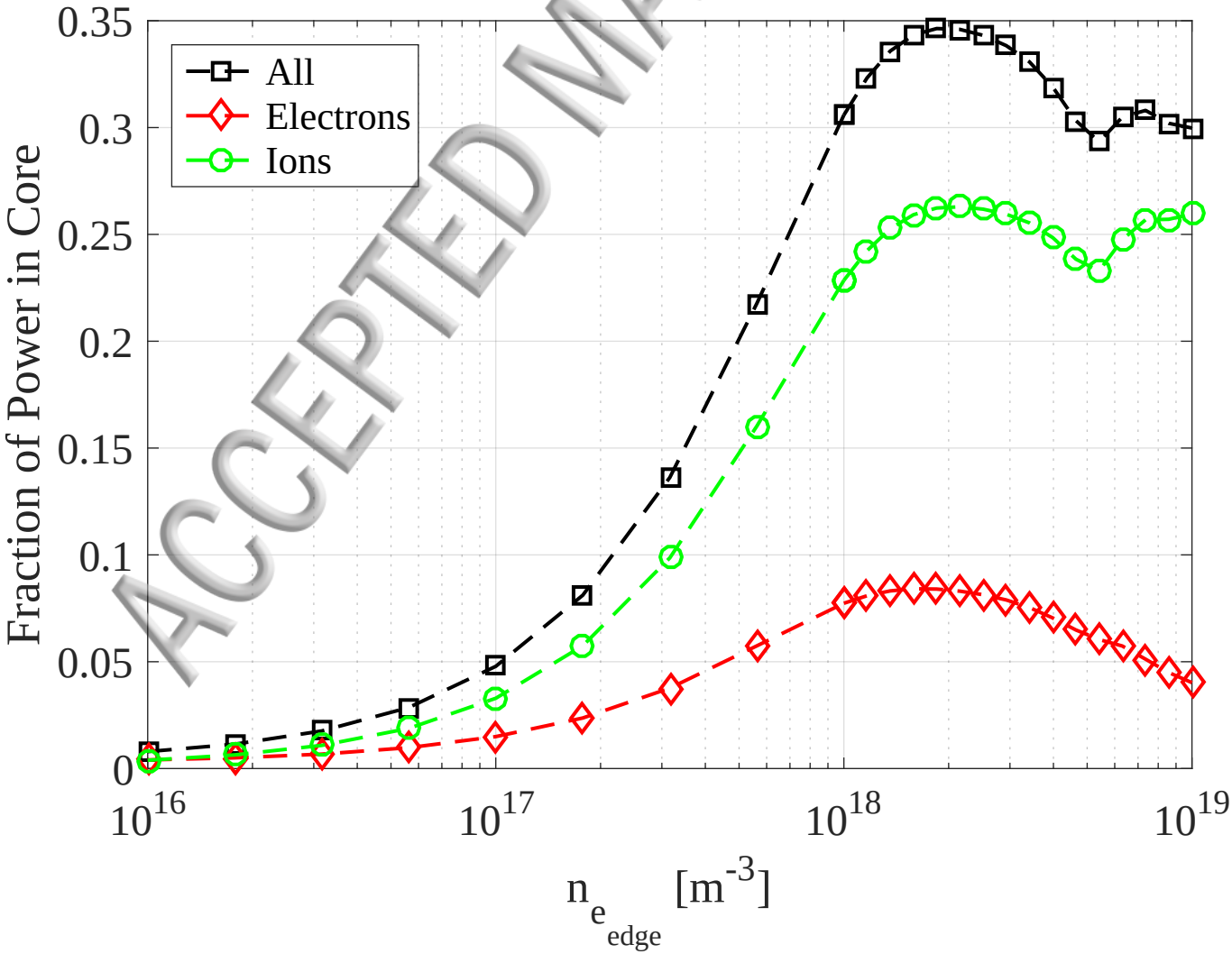
All
Electrons
Ions
Fraction of Power in Core
0.35
0.3
0.25
0.2
0.15
0.1
0.05
0
10^{16}
10^{17}
10^{18}
10^{19}
$n_{e_{edge}}$ [m^{-3}]